Journal of Astronomical Telescopes, Instruments, and Systems

AstronomicalTelescopes.SPIEDigitalLibrary.org

Zero dark current in H2RG detectors: it is all multiplexer glow

Michael W. Regan
Louis E. Bergeron

SPIE.

Michael W. Regan, Louis E. Bergeron, "Zero dark current in H2RG detectors: it is all multiplexer glow," *J. Astron. Telesc. Instrum. Syst.* **6**(1), 016001 (2020), doi: 10.1117/1.JATIS.6.1.016001

Zero dark current in H2RG detectors: it is all multiplexer glow

Michael W. Regan* **and Louis E. Bergeron**
Space Telescope Science Institute, Baltimore, Maryland, United States

Abstract. We present the analysis of James Webb Space Telescope near-infrared H2RG detectors with a 5-μm cutoff, which shows that, at temperatures <60 K, there is no measurable dark current. Instead, the observed signal in dark exposures is almost entirely due to multiplexer glow that arises as each pixel is selected. We are able to separate the per-sample glow from the time-dependent dark current by comparing the observed signal in both continuous and sparsely sampled dark exposures. Such explicit tests are required to break the degeneracy between dark current and uniform amplifier glow. We show that the glow is lower within the regions of the detector that are missing the epoxy back fill (voids). We also find that the glow from each pixel extends out to a radius of several pixels. Because of the higher sampling frequency of subarray observations, the per-sample glow leads to a higher apparent dark current in subarray exposures. Finally, we show that the magnitude of the glow is affected by the pixel source follower current, the pixel clocking rate, and the number of outputs running in parallel. Our measurement of an insignificant dark current shows that the detector noise is no longer limited by the quality of the mercury cadmium telluride layer but instead by the multiplexer and readout electronics.
 [DOI: 10.1117/1.JATIS.6.1.016001]

Keywords: infrared detectors; James Webb Space Telescope; multiplexer glow; dark current; self heating; mercury cadmium telluride.

Paper 19075 received Jul. 2, 2019; accepted for publication Jan. 30, 2020; published online Feb. 19, 2020.

1 Introduction

The long-wavelength sensitivity of infrared detectors makes them susceptible to self-generated emission sources.[1] In a dark exposure, the emission from these sources can lead to a glow that is significant compared to the dark current, lowering the sensitivity of these detectors in low background fields. Because infrared detectors use readout integrated circuits (ROICs or multiplexers) that are capable of nondestructively sampling the pixels in an up-the-ramp (UTR) exposure,[2] the number of samples in a single exposure can be in the 100s to 1000s leading to a high sensitivity to a per-sample glow. In previous studies, the sources of glow have been primarily attributed to amplifiers on the perimeter of the detectors. We show this example in a Hubble Space Telescope Near-Infrared Camera and MultiObject Spectrometer (NICMOS) channel 3 dark exposure; see Fig. 1. Here, the four corners of the detector have a much higher signal than the center of the detector due to the amplifier glow. Because NICMOS had a variety of readout modes with different intervals between the samples, it was possible to show that there was a linear relationship between the observed amplifier glow and the number of samples in the exposure rather than the exposure time. Alternatively, if the amplifiers had been continuously glowing, the total signal from them would have been proportional to the exposure time.

Preventing amplifier glow from affecting the detectors has been a goal of detector developers, but even today newly developed detectors can show significant amplifier glow.[3] The H2RG detectors developed for the James Webb Space Telescope (JWST) by Teledyne[4,5] have a long heritage tracing back to the NICMOS detectors. Over time, Teledyne has been able to design ROIC to be able to block the light path from the offchip amplifiers to the detector layer. Figure 2 shows an example of H2RG dark slope image that was formed from the median of twenty-five 300-frame (~3300 s) UTR exposures. (In a UTR exposure, note that a frame is a single sample

*Address all correspondence to Michael W. Regan, E-mail: mregan@stsci.edu

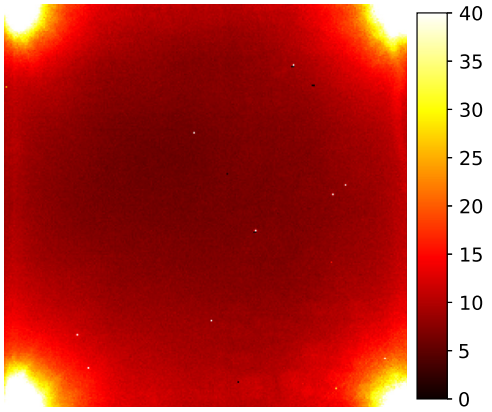

Fig. 1 The per-sample glow of the channel 3 NICMOS detector on the Hubble Space Telescope. The units are in electrons per sample. The strong glow from the offchip amplifier at each corner leads to a minimum per-sample glow of six electrons. Note that high count rates at the edge of the detector near the amplifiers are the expected signature of amplifier glow.

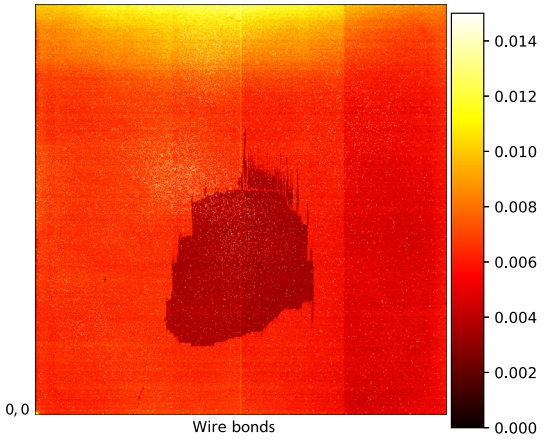

Fig. 2 A slope image formed from the median of twenty-five 300-frame UTR continuously sampled dark exposures with the detector at 37 K. The pixels at the center of the image with significantly lower slopes are found where there is a void in the epoxy underfilled between the multiplexer and the mercury cadmium telluride (HgCdTe) layer.[6] The region at the top with a higher slope is opposite the side of the detector with the wire bonds. Because this feature was not seen in earlier testing of this detector,[6] it is not intrinsic to the device. It is possible that this is due to a reflection coming from below the detector mount. A very small region of enhanced slope can be seen in the lower left corner. This may be due to something in the multiplexer. The total exposure time is 3300 s. The slope is in units of $e^{-}s^{-1}$. The lower left corner is the first pixel sampled (0, 0) and the fast scan direction is horizontal.

of all the pixels. The time to sample all the pixels in a frame is the frame time.) The image shows almost no signs of offchip amplifier glow. There is a very small region in the lower left that might be due to something in the multiplexer.

Testing of the JWST Near-Infrared Imager and Slitless Spectrograph subarray darks showed that in dark exposures the observed count rate in $e^{-}s^{-1}$ varied significantly depending on the size of the subarray. The apparent dark current was unexpectedly high in the small subarrays compared to the full-frame rate. However, the results are consistent with a constant rate measured in terms of electrons/frame independent of array size from the smallest subarray of 80×80 up to the full frame of 2048×2048. This range in frame sizes leads to a factor of $\sim$150 in time per-frame. The almost constant rate per-frame could only be explained by a per-frame signal that is significantly higher than the actual dark current.

We present lab results where we separate the two contributors to the observed dark slope images: the dark current and a per-frame multiplexer glow. We show that the per-frame glow

is generated within the multiplexer as each pixel is selected. We also show that this glow is the sole contributor to the dark slope at temperatures <60 K and reveal what parameters affect the magnitude of the glow.

2 Separating the Per-Frame Signal (Electrons/Sample) from the Dark Current (Electrons/Second)

To separate the dark current per-time and the glow per-sample from a dark slope image, we used a flight batch JWST H2RG detector, 17166. This is a near-infrared spectrograph 5-μm cutoff device that was part of the flight generation of detectors fabricated for JWST.[6] The JWST H2RG detectors are all read out using System Image, Digitizing, Enhancing, Controlling, and Retrieving (SIDECAR) Application Specific Integrated Circuits[4] running the flight JWST SIDECAR software. The relationship between measured slope S, exposure time t, dark current D, number of frames in the exposure N_f, and per-frame glow F is

$$S = (FN_f)/t + D.$$

The problem is that all of the JWST readout patterns continuously clock the array leading to a degeneracy between a per-sample signal and a per-time signal.

To break this degeneracy, we created a sparse sampling readout pattern that completely pauses the clocking of the detector between successive frames of the array using the single-step mode in the flight SIDECAR software. (In the JWST flight software, this can also be implemented using drop frames set to "no clocking.") All of the sparse exposures here are taken with the clocking paused for two frame times between samples. For our initial measurement with the detector at 37 K, we took sets of 25 UTR exposures with 300 frames in the standard continuous sampling mode (3300-s exposure time) and a matching set of 25 UTR exposures with 100 frames of sparse sampling in single-step mode (also 3300-s exposure time). Although we would expect that in the sparsely sampled exposures, there would be some thermal effects in the detector caused by the variation in dissipation between clocking the array and letting it sit idle; the effects will be the same for each sample in the exposure and thus should not affect the measured slopes.

Figure 3 shows the slope images for the continuous UTR 300 and sparse UTR 100 exposures. Because the total exposure time is the same in the UTR 300 and UTR 100 exposures, the higher slope seen in the UTR 300 exposure [Fig. 3(a)] compared to the UTR 100 exposure [Fig. 3(b)] must be due to the extra 200 samples of the pixels in the UTR 300. There is clearly a large per-frame component of the slope. The large epoxy void area is also evident, with a significantly lower signal inside the void.

Using the continuously sampled UTR 300 and sparsely sampled UTR 100 images, we solved for F and D for each pixel, allowing us to separate the per-frame glow component from the

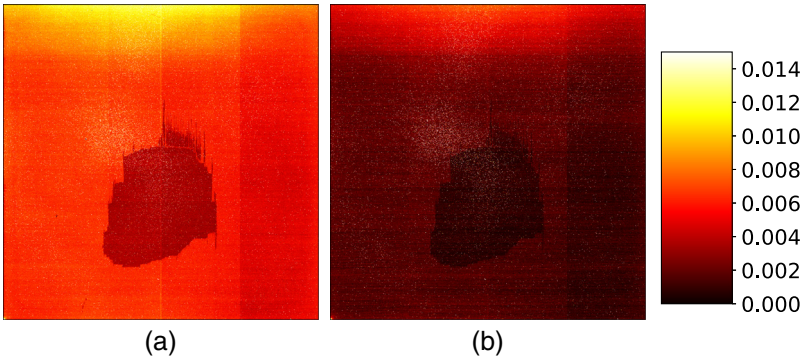

Fig. 3 Median slope image from (a) a UTR 300-frame continuously sampled dark and (b) a UTR 100-frame sparsely sampled dark. The two images have the same total exposure time. The slope in the sparsely sampled image is significantly lower than in the continuously sampled image. This is a strong evidence for a large per-frame contribution to the slope. The detector was at 37 K and the slopes are in units of $e^{-}s^{-1}$.

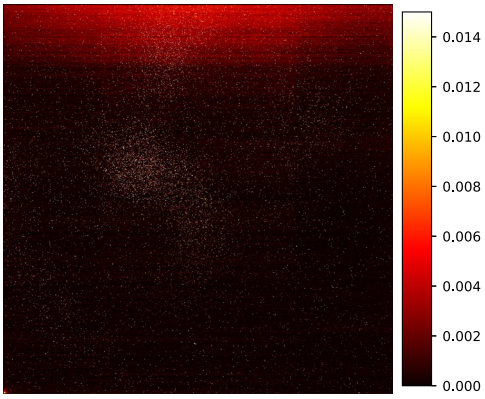

Fig. 4 The dark current component of the 37-K slope image in units of $e^{-}s^{-1}$. This reveals that the enhanced rates at the top and lower left corners of the detector are proportional to time and not number of samples. The only other feature in the image is the hot pixels. The vast majority of the pixels have dark currents that are below our detection limit. The other striking feature is the complete lack of any sign of the void region.

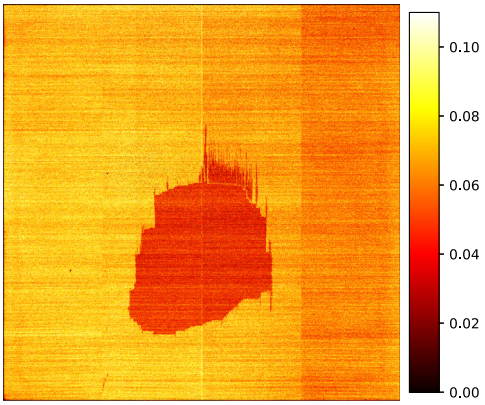

Fig. 5 The per-frame signal (electrons/frame) of the 37-K slope image. Here, the void is strongly visible. In addition, we do not see the hot pixels or the glow at the top of the detector that appears in the dark current image.

time-dependent dark current component. Figure 4 shows the dark current. The void is undetectable, and over the majority of the array, the dark current is zero within the noise. The only components that are a function of the exposure time are the glow at the top of the array and the hot pixels.

Figure 5 shows the derived per-frame signal. The most striking feature in the per-frame signal is the void. The per-frame signal outside the void is 0.076 electrons per-frame while within the void, the signal is significantly lower, i.e., 0.045 electrons/frame. The fact that the per-frame signal is affected by the presence of the epoxy between the multiplexer and the detector layer is evident that this effect is caused by a glow in the multiplexer. If the signal was due to each sample ejecting a residual charge into the pixel, it would not depend on whether or not there is epoxy between the multiplexer and the detector layer. In that case, the charge would travel via the electrical connection between the multiplexer and the detector layer, which is unaffected by the presence of epoxy. It seems counterintuitive that the glow is higher when there is epoxy between the multiplexer and the detector layer. It could be that the epoxy has a better match to the index of refraction of the multiplexer limiting the internal reflection at the surface.

2.1 *Dark Current as a Function of Temperature*

Figure 4 shows the dark current image that only contains the hot pixels and the emission at the top of the detector. To better test the algorithm, we repeated the experiment with the detector at

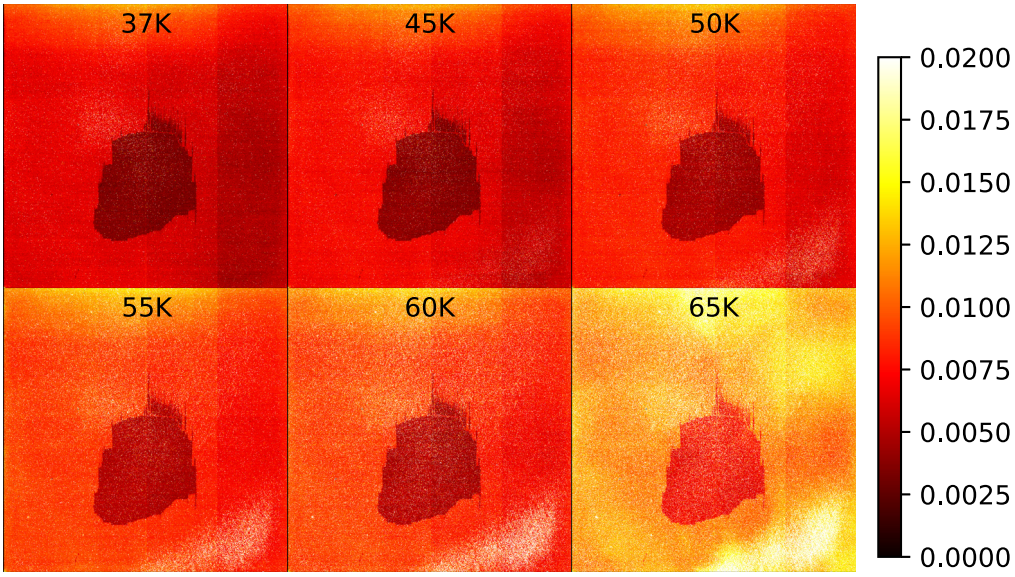

Fig. 6 Median slope images from the set of dark exposures taken at a range of temperatures. Other than the significant increase in fraction of hot pixels, only the 65-K slope image shows a significant change. The units are $e^{-}s^{-1}$.

a range of temperatures to confirm that the algorithm is correctly separating out the dark current and the per-frame glow in the dark exposures. As we increased the temperature, we expected to see a strong contribution from the thermally generated dark current appearing in all the pixels starting around 45 K.[7]

Figure 6 shows the median slope images from the sets of 25 continuous UTR 300 dark exposures at temperatures from 37 to 65 K. From theses images and matching sparse UTR 100 images, we separated the dark current and per-frame components. We show these in Figs. 7 and 8, respectively. Despite an increase in the number of hot pixels, the dark current remains around zero until the detector is >55 K. As expected, the per-frame glow is almost unchanged with changing temperatures. The clear separation of the dark current from the per-frame glow

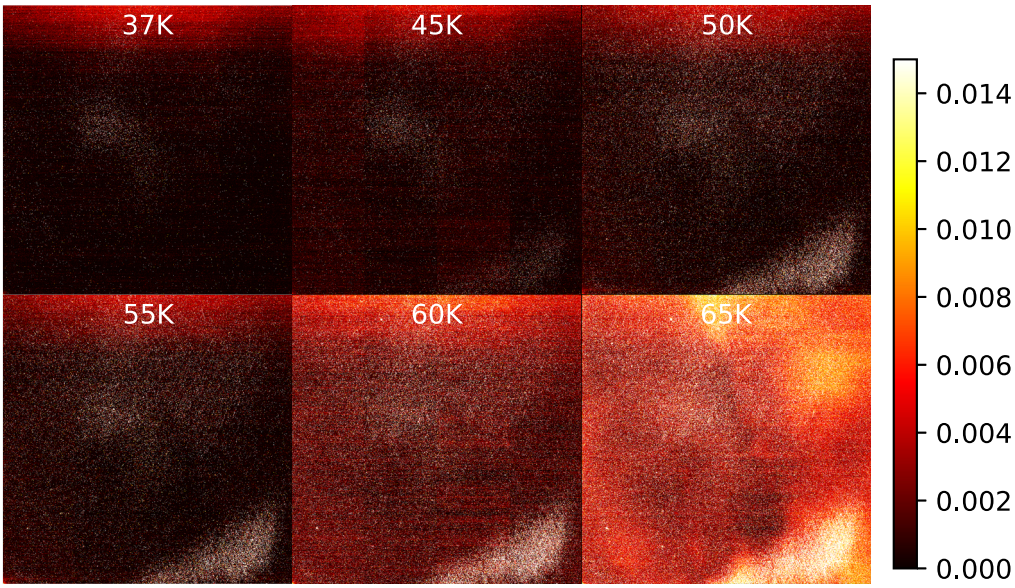

Fig. 7 The derived dark current with increasing temperatures. Note that the void does not appear at any temperature. The units are $e^{-}s^{-1}$.

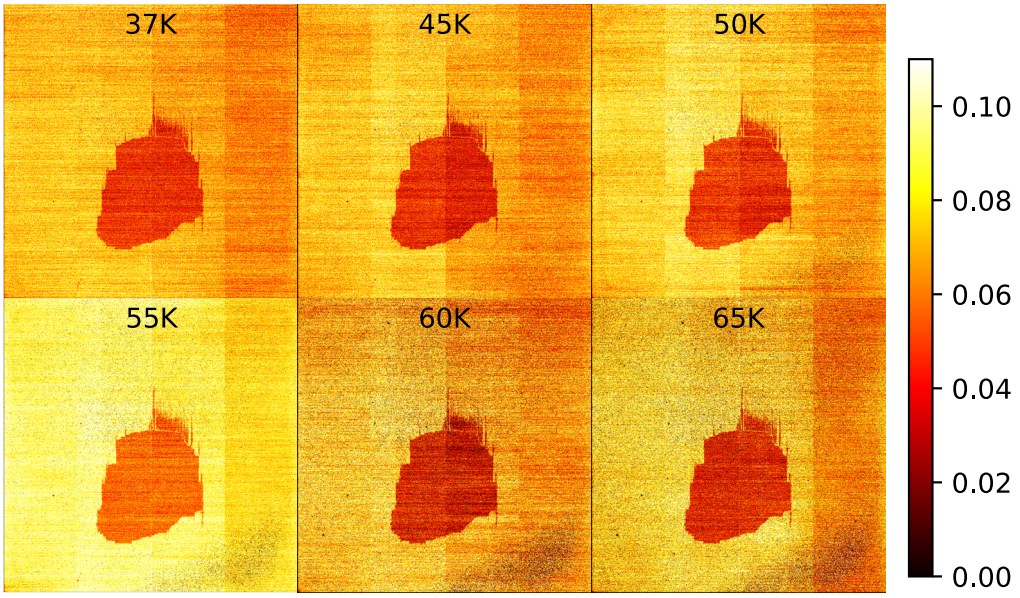

Fig. 8 The per-frame glow at a range of temperatures. The void is again clearly seen here. As expected, both the hot pixels and reflected glow are not seen here. The magnitude of the per-frame glow does not change as the temperature increases. Note that hot pixels that saturate appear as dark pixels since the separation of dark current and glow is not possible with saturated pixels.

over this range of temperatures confirms that the algorithm for separating the two terms is correct.

We plot the median of the dark current as a function of temperature in Fig. 9. The figure shows that the dark current is nearly zero <60 K. The weighted mean dark current for the five measurements <60 K is 8×10^{-6} $e^{-}s^{-1}$. The one-sigma uncertainty of the mean is 2×10^{-4} $e^{-}s^{-1}$. Even at 60 K, the small measured dark current could be due to the large fraction of hot pixels biasing the median. Only the 65-K dark current image shows any large scale structure in the dark current, and at that relatively warm temperature, we may actually be detecting thermal emission (see Sec. 4.1).

We can better view the pixel distribution of the dark current values in Fig. 10. The histogram shows that the mode of the dark current is constant until the temperature reaches 60 K. We can better see the effect of increasing temperature on the hot pixel fraction in Fig. 11 where we show the fraction of hot pixels as a function of temperature in a format similar to that of the study by Rauscher et al.[7] This shows that even at 65 K, the fraction of operable pixels remains over 80%.

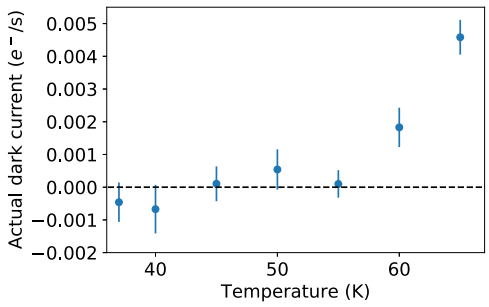

Fig. 9 Median value of the dark current as a function of temperature excluding the outer 200 pixels on all sides. Note that the dark current at 55 K and below is zero within the measurement error. The measurement at 60 K could have a positive bias due to the large number of hot pixels at that temperature. The error bars are one sigma derived from the variance of the median dark slopes for the continuous and sparse exposures used.

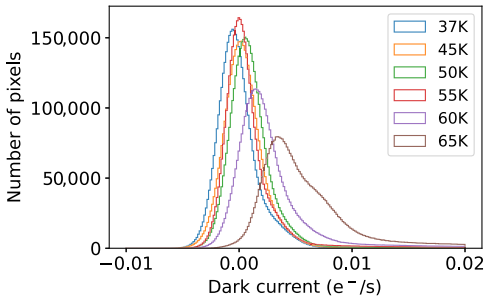

Fig. 10 The number of pixels with the measured dark current for six different temperatures. The dark current is measured in $e^{-}s^{-1}$.

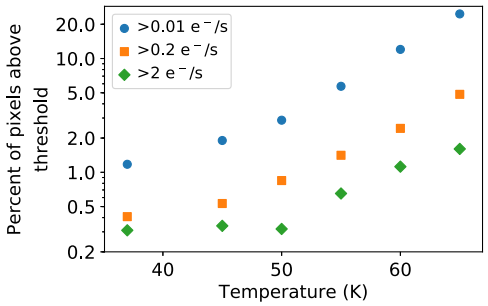

Fig. 11 The fraction of pixels above three different thresholds (0.01 $e^{-}s^{-1}$, 0.2 $e^{-}s^{-1}$, and 2 $e^{-}s^{-1}$) at varying detector temperatures similar to the study by Rauscher et al.[7] While the number increases substantially between 37 and 65 K, up to 50 K, the hot-pixel fraction is still only around 3%.

3 Characteristics of the Multiplexer Glow

3.1 *Glow Spread Function*

When testing using the improved reference sampling and subtraction (IRS^2) readout mode,[8] we noticed that the measured slope in dark exposures was higher in the pixels adjacent to the bottom reference pixels that are multiply-sampled in the IRS^2 mode. This implied that the glow generated when a pixel is sampled is not confined to the pixel itself.

To investigate this, we set up an experiment using a single-pixel subarray observing in the H2RG window mode. The experiment used four single-pixel subarrays, one in each amplifier. To vary the fast scan direction, we located the four subarrays in different quadrants of the array; this gave us the first and third subarray samplings from left to right and the second and fourth samplings from right to left. We positioned the first and fourth subarrays outside of the void region and the second and third subarrays inside the void. We chose the subarray locations to avoid nearby hot pixels to prevent them from interfering with the glow measurement. We configured the detector to use a high source follower current for this exposure to increase the glow (see Sec. 3.2.1) and thus the signal-to-noise ratio of the measurement.

To measure the effect of the glow on nearby pixels, we wanted a full-frame image with only a few full-frame samples (to minimize the glow from the pixels outside of the single-pixel subarrays) but with a large number of samples of the single-pixel subarrays (to maximize the glow from the single-pixel subarrays). To accomplish this, we first turned off idle-mode resetting so that there was no sampling or resetting during the idle period. Then, we performed a single full-frame pixel-by-pixel reset of the entire array. Next, we started the exposure with five full-frame samples. Then, while the detector was sitting idle, we addressed each subarray in turn and took a subarray ramp exposure with NO reset but with a very large number of samples. We accomplished this by taking a UTR exposure with 11 returned samples; however, between each sample that was returned to the data acquisition computer, we performed an additional 4000 samples of

the pixel that were not returned. (This is the drop2 parameter for JWST.) This resulted in $(11-1)\times 4000+(11)=40{,}011$ samples of that single-pixel subarray and took ~21 s of wall clock time. We then repeated this for the other three subarrays. Figure 12 shows a schematic of the readout pattern, the readout directions, and the locations of the subarrays. After a set of subarray samples had been completed (~90 s of wall clock time), we switched back to full-frame mode and obtained five full-frame samples without resetting. We repeated the set of subarray and full-frame samples two more times to obtain a total exposure that had four full-frame sets of five samples UTR and a total of three ramps for each single-pixel subarray resulting in $40{,}011\times 3=120{,}033$ samples of each of our single-pixel subarrays in ~5 min of wall clock time. We then processed the full-frame ramp and fitted a per-frame slope for each pixel.

We cut out 20×20 pixel subsections from the resulting full-frame slope image surrounding each of the single-pixel subarrays. We show these in Fig. 13, along with a horizontal row slice through the center. The illumination from the glow, the glow spread function (GSF), clearly extends several pixels beyond the pixel being sampled (marked with the green cross) and is asymmetric in the horizontal direction—independent of the readout direction. It appears to have the same characteristic shape everywhere on the detector with the GSF amplitude being lower inside the void. The shape is likely due to the geometry of the glow source in the multiplexers unit cell, combined with interactions with the indium bumps and the back-fill epoxy.

We conclude that the uniform glow amplitude seen in full-frame exposures is actually the sum of the GSF emission from all the nearby pixels. The same is true for subarray exposures except that there is no glow contribution from the pixels outside the subarray (which are not being sampled). This implies that there should be a border of apparently lower glow signal around the perimeter of subarrays. Figure 14 shows a UTR 300 dark slope image of a 100×100 subarray. As expected, we do see a dark pixel border around the subarray. We convolved a unity square with the GSF and compared it to the actual subarray glow and the match is excellent along the top and bottom, with some interesting additional features along the left and right edges, which we are currently investigating. Note that although the reference pixels do not accumulate any glow signal, sampling the reference pixels produces glow just like the data pixels. Any pixels adjacent to reference pixels being sampled will indeed detect their glow. This explains the higher

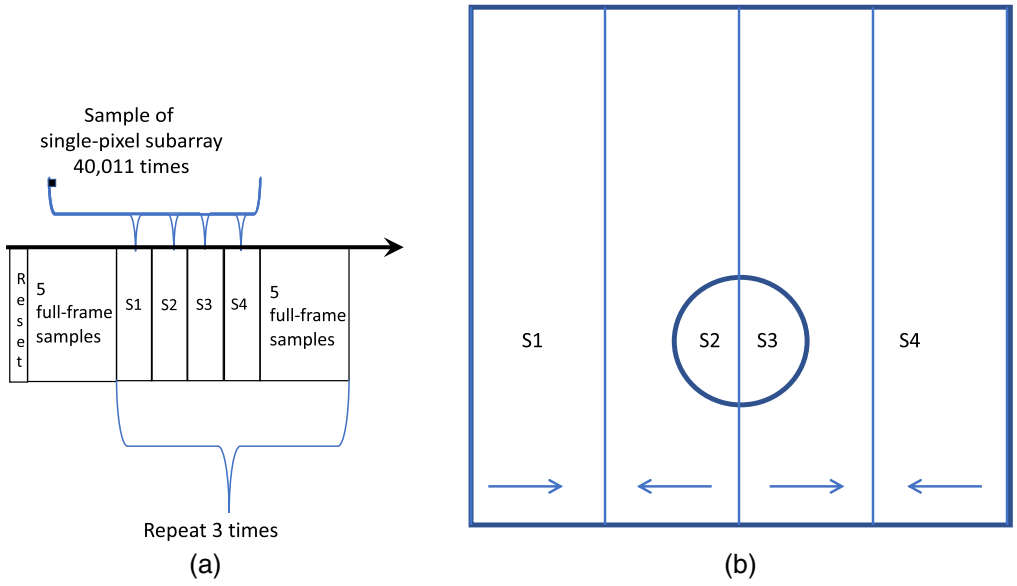

Fig. 12 (a) A schematic diagram of how the single-pixel subarrays were sampled compared to the full frame. First, we perform a full-frame reset and then we obtain five full-frame samples. We then sample each single-pixel subarray (S1 to S4) 40,011 times. After each single-pixel subarray has been sampled, we obtain five full-frame samples. We repeat the single-pixel ramps and full-frame samples two more times to create the final dataset. (b) The locations of the single-pixel subarrays relative to the void (central circle) and the readout directions (arrows at the bottom).

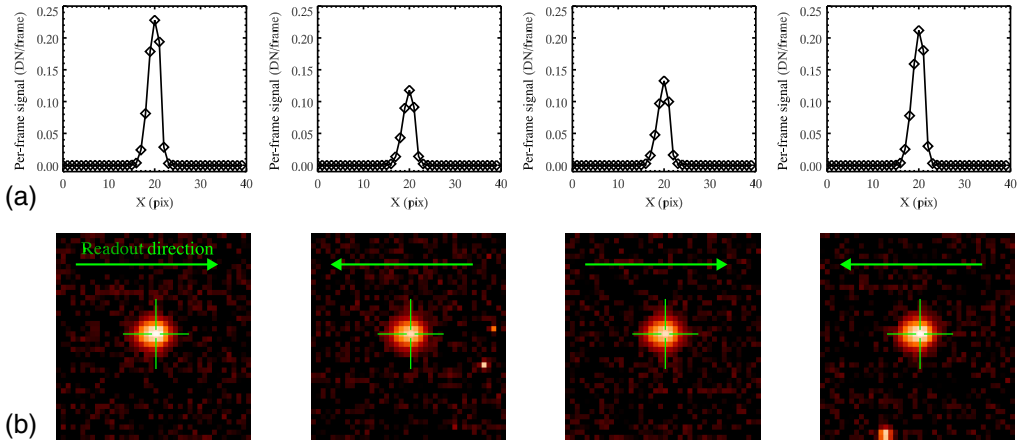

Fig. 13 GSF for the four single-pixel subarrays. (a) The magnitude of the glow in a slice along the middle row of the subarray. (b) A log stretch of the GSF. The figures show that the GSF is asymmetrical with a bias to the right. This asymmetry does not depend on the read direction. We can also see that the magnitude of the glow is lower inside the void.

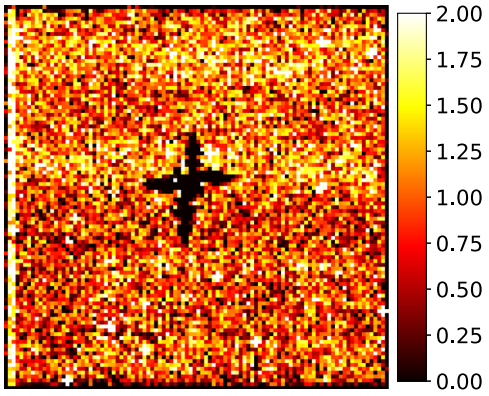

Fig. 14 A single 100×100 UTR 300 dark slope image (~34-s exposure time) taken with a high-pixel source follower current to increase the signal-to-noise ratio of the glow. The pixels on the edges of the subarray show a significantly lower slope due to the lack of any glow contribution from their neighbors outside of the subarray. Note that the second and third columns from the left show an increased slope value. We do not know about this cause, but it switches to the other side of the subarray when we change the direction of the sampling to be from the right to the left rather than the default of left to right. The dark cross in the center of the image is an epoxy void. The units of the image are electrons/frame.

slopes that we observed in pixels adjacent to the reference pixels that are multiply-sampled in the IRS^2 dark exposures.[9]

3.2 *Glow Dependencies*

At least three things affect the magnitude of the per-sample glow: pixel source follower current, number of simultaneous outputs being used, and pixel clocking rate.

3.2.1 *Pixel source follower current*

In previous studies, we found that, as we increase the pixel source follower current, the apparent dark current increases. On the other hand, lowering the current available to the pixel source follower led to a longer analog signal-settling time. The most obvious sign of this is an asymmetry in the fast-read direction of the signal of pixels adjacent to hot pixels. Without enough current, pixels

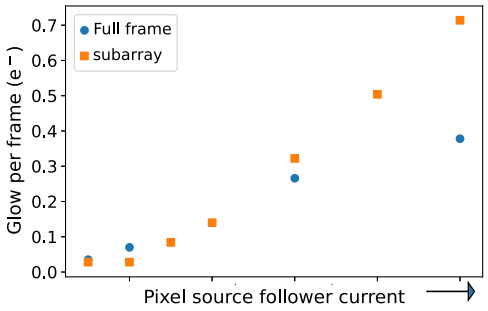

Fig. 15 The measured per-frame glow as a function of the current provided to the pixel source follower for both full frame and subarray. Note that, at higher current levels, the per-frame glow in subarray is a factor of two higher than in full frame.

that are immediately sampled after hot pixels will not be fully settled and will have a higher signal than pixels that are sampled immediately before the hot pixels. This magnitude of the asymmetry depends on both the available pixel source follower buffer drive current and the slew rate resulting from the wiring harness between the H2RG detector outputs and the readout electronics. As a result, when optimizing the readout electronics, there has always been a trade-off when choosing the pixel source follower current between a lower apparent dark current and poor analog settling. Even though this increase in the apparent dark current as the source follower current was increased was not consistent with the dark current being a characteristic of the HgCdTe detector layer.

By separating out the dark current and the per-frame glow, we found that, as the source follower current is increased, the dark current remains constant (near zero), but the per-frame glow increases. Figure 15 shows how the full-frame per-frame glow increases as the source follower current increases. This result resolves the incongruity of apparent dark current changing with source follower current.

3.2.2 *Number of simultaneous outputs*

Another interesting result is that, at high current settings, the glow is significantly higher in subarrays than full frame at the same current setting. For JWST, the H2RG standard subarrays are read out in "window mode" that uses a single output to read out the subarray. This is different from the standard JWST full-frame readout that uses four outputs. Because the number of simultaneous outputs being used was the only difference that we could find between the way the two modes are sampled, we decided to go to the other extreme and measure the per-frame glow using 32 outputs. While the harness we used is not wired to send the 32 outputs to the SIDECAR, we can still perform the exposures using 32 outputs. The lack of connections results in the output image containing only samples for $1/8$ of the pixels with the rest being blank. Our analysis of the glow from the 32 output mode exposures showed that the per-frame glow was a factor of 2.5 lower than the standard four output full-frame exposures. This implies that, even though the supplied current is the same between the three setups, the effective current being provided to each pixel that affects the glow seems to be dependent on the number of outputs being used. We looked at the settling between full-frame and subarray exposures at the same low source follower current but found no differences in the asymmetries of the pixel adjacent to the hot pixels.

3.2.3 *Pixel clocking rate*

We also measured the glow as a function of the pixel-selection time. Figure 16 shows the per-frame glow at various pixel dwell times for full-frame exposures. The figure clearly shows that the glow is directly proportional to the amount of time that the pixel was selected.

3.3 *Wavelength of the Per-Frame Glow*

H2RG detectors with two different wavelength cutoffs are being used in the JWST Near-Infrared Camera (NIRcam): one with a 5-μm cutoff and one with a 2.5-μm cutoff. Measurements of the

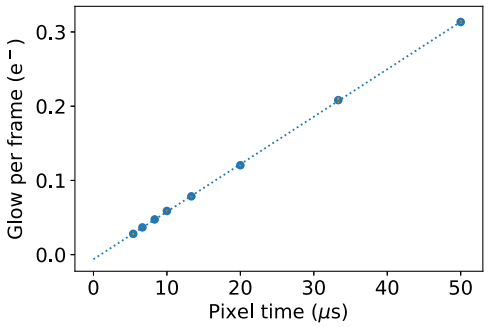

Fig. 16 The measured per-frame glow as a function of the pixel clocking time. This is the amount of time that a pixel is selected (the inverse of the pixel clocking rate). The dotted line is a least squares fit to the values. The linear relationship implies that the pixel glows for the duration of the time that it is selected. The one-sigma error bars are smaller than the symbol sizes.

apparent dark current have consistently shown a significantly lower value for the 2.5-μm cutoff devices (<0.001 e^-s^{-1})[10] than the 5-μm cutoff devices. Given that we have shown here that the dark current is near zero, this lower apparent dark current implies that there is a significantly lower per-frame glow in the short wavelength cutoff detectors. Thus, the vast majority of the glow must come from wavelengths >2.5 μm. This strong wavelength dependence is consistent with the source of the emission being hot-electron bremsstrahlung.[1]

4 Discussion

4.1 *Is There Dark Current at 65 K?*

It is still not conclusive that there is dark current even at 65 K. Figure 17 shows empirical relationship (rule 07) between dark current density and the cutoff wavelength of HgCdTe detectors.[11] It shows that the expected dark current density is about a factor of 3 below the value that we observe. The high fraction of hot pixels makes it difficult to find pixels that are not affected by hot pixels. In addition, the overall morphology of the dark current in Fig. 7 is similar to the pattern in the slope images when we are cooling down to the operational temperature. Figure 18 shows a slope image taken during a cooldown with the warm blank in front of the detector. The image shows the same basic morphology as in the 65-K slope image. To find the thermal emission threshold during a cooldown, we moved a thermistor to the back of the blank and varied the temperature of the blank while holding the detector at 37 K. We found that we could not detect the emission from the blank <68 K. However, above this temperature, the emission pattern shown in Fig. 18 begins to appear and increases in intensity with temperature. We see a similar but morphologically unique pattern in other H2RG and H4RG devices when they are detecting thermal emission.

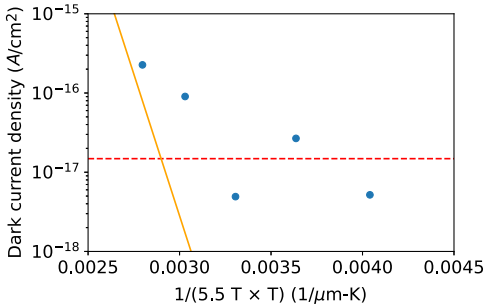

Fig. 17 The blue points are our dark current density measurements as a function of the reciprocal of the cutoff wavelength (5.5 μm) times temperature. The solid orange line is the "rule 07"[11] expected dark current density for this cutoff wavelength. The dashed line is the detection threshold of our dark current density measurements.

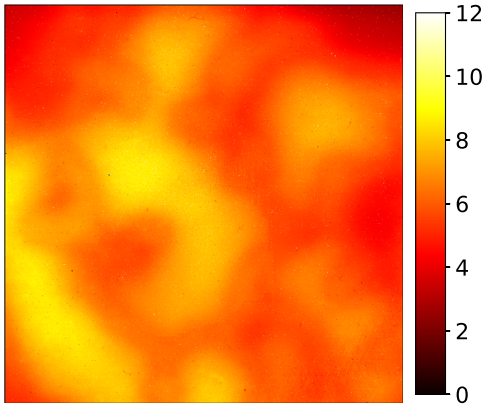

Fig. 18 A dark slope image during a cooldown when the detector is at an operating temperature of 37 K, but the blank in front of the detector has not cooled down and is still at ~75 K. This overall morphology is very similar to what we see in the 65-K dark slope image (Fig. 7). The units are in $e^{-}s^{-1}$.

Given that when the detector is at 65 K there is only a small difference between the detector temperature and the thermal emission threshold, it is hard to rule out that what we are seeing at 65 K is not some form of thermal emission. At some level, it does not matter because at 65 K we are clearly too close to detecting thermal emission and the hot pixel fraction is significant. Even so, it is interesting that this cutoff wavelength yields a prediction that the dark current is only marginally detectable near the temperature at which thermal radiation from the enclosure becomes significant.

4.2 *Why Has This Not Been Seen Before?*

There are several factors that may have prevented this effect from being found earlier. The first is that the glow is uniform over the detector rather than emanating from point-like sources at the edges of the detector, such as the NICMOS detector in Fig. 1. Another cause is that with only a single method of sampling the detector, it is not possible to distinguish between light leaks, dark current, and uniform multiplexer glow. For example, Blank et al.[5] attribute the floor in the apparent dark current at low temperatures seen in 2.5-μm cutoff H2RG detectors to "background light or testing limitations." Furthermore, the theoretical additional sources of dark current such as generation recombination and surface currents that do not depend on temperature have provided an explanation for the observed floor in dark current values below some temperature.[7] Explicit tests are required to break the degeneracy between dark current and uniform amplifier glow. For example, Smith et al.[12] used a method similar to ours to determine the multiplexer glow in a VIRGO-2K 2.5-μm cutoff device and found a per-sample glow of 0.04 e^{-}/frame. Even after removing this component, they still had a significant dark current in their engineering grade device.

4.3 *What are the Implications of No Dark Current and Only Multiplexer Glow?*

There are several implications of the dark current being near zero <60 K. The first is that for instruments where the noise is dominated by the apparent dark current, readout patterns other than continuous sampling could lead to lower noise. The JWST mode of continuous sampling leads to the highest possible amount of glow per unit time. An alternative readout pattern similar to our sparse sampling readout would decrease the electrons deposited in the pixels by the multiplexer glow. The trade-off is that the lower number of samples would increase the effective read noise. For instruments with a low per-pixel background and with low read noise, sparse sampling would yield a higher signal-to-noise ratio than continuous sampling.

In addition, for JWST, it provides some margin on the usable operating temperature of the detectors during the mission. Over the life of the mission, the sun shield on JWST will degrade as

micrometeors create holes in the thin Kapton membranes of the sun shield. This will cause the temperature of the telescope and instruments to increase throughout the mission. This fact is accounted for in the mission models but our finding of a lower sensitivity to increased temperature will add extra margin. While the increasing temperature will increase the number of hot pixels, we have shown that the dark current of the nonhot pixels remains unchanged up to 60 K. The higher hot pixel fraction could be mitigated by a revised observing strategy that increases the number of dither locations for each pointing.

The longer-term significance is that when the dark current is as low as we have measured, the characteristics of the HgCdTe layer are no longer a major issue in the noise characteristics of the detectors (it still is important for persistence). Instead, the multiplexer and readout electronics become the major sources of noise. This is encouraging for future progress because these use commercial fabrication techniques rather than the specialized manufacturing process required for HgCdTe detector layers. This opens up the possibility of cost-effective enhancements.

Finally, the lower per-frame glow when 32 outputs are used is a potential incentive to use more outputs when the extra thermal load of using 32 outputs is not an issue.

5 Conclusions

The measured slope in dark images <60 K is almost entirely due to the per-frame glow from the multiplexer. This implies that the dark current of 5-μm cutoff H2RG detectors has been significantly overestimated. While this result is for a single detector, the measured apparent dark current for the device is basically the same as all other JWST 5-μm cutoff detectors.[6] Thus, the dark current on the other devices should be equally low. Even with the settings that lead to the lowest glow at 37 K, practically all of the accumulated electrons in the 3300-s exposures are coming from the per-frame glow. In fact, the dark current is consistent with zero <60 K.

The epoxy void only shows up in the per-frame component. This should be expected because the dark current in the detector should not be affected by the void. The lower glow in the void implies that the epoxy between the multiplexer and the HgCdTe layer changes the optical characteristics of the multiplexer surface allowing more light to escape and increasing the per-frame glow.

The measured dark slopes in subarrays are significantly higher than the full-frame exposures due to the higher number of samples per unit time. Moreover, the slopes at the edges of the subarrays are always lower due to the lack of a glow contribution from pixels outside of the subarray.

Sampling the reference pixels leads to glow and thus the data pixels adjacent to reference pixels will be affected. This glow can be significant when the reference pixels are sampled at a high frequency such as in IRS^2 mode and in the equivalent mode of the H4RG.

Finally, the amount of glow generated per sample can be decreased by decreasing the pixel source follower current, increasing the pixel clocking rate, and increasing the number of outputs that are sampled simultaneously.

References

1. S. Tam and C. Hu, "Hot-electron-induced photon and photocarrier generation in silicon MOSFET's," *IEEE Trans. Electron Devices* **31**, 1264–1273 (1984).
2. J. D. Garnett and Forrest W. J., "Multiply sampled read-limited and background-limited noise performance," *Proc. SPIE* **1946** (1993).
3. O. Boulade et al., "Development activities on NIR large format MCT detectors for astrophysics and space science at CEA and SOFRADIR," *Proc. SPIE* **9915**, 99150C (2016).
4. M. Loose et al., "HAWAII-2RG: a 2k × 2k CMOS multiplexer for low and high background astronomy applications," *Proc. SPIE* **4850**, 867–879 (2003).
5. R. Blank et al., "H2RG focal plane array and camera performance update," *Proc. SPIE* **8453**, 845310 (2012).
6. B. J. Rauscher et al., "New and better detectors for the JWST near-infrared spectrograph," *Publ. Astron. Soc. Pac.* **126**, 739 (2014).

7. B. J. Rauscher et al., "The dark current and hot pixel percentage of James Webb Space Telescope 5 μm cutoff HgCdTe detector arrays as functions of temperature," *Publ. Astron. Soc. Pac.* **123**, 953–957 (2011).
8. B. J. Rauscher et al., "Reducing the read noise of HAWAII-2RG detector systems with improved reference sampling and subtraction (IRS^2)," *Proc. SPIE* **8453**, 84531F (2012).
9. B. J. Rauscher et al., "Improved reference sampling and subtraction: a technique for reducing the read noise of near-infrared detector systems," *Publ. Astron. Soc. Pac.* **129**, 105003 (2017).
10. C. A. Beichman et al., "Science opportunities with the near-IR camera (NIRCam) on the James Webb Space Telescope (JWST)," *Proc. SPIE* **8442**, 84422N (2012).
11. W. Tennant et al., "MBE HgCdTe technology: a very general solution to IR detection, described by 'rule 07', a very convenient heuristic," *J. Electron. Mater.* **37**, 1406–1410 (2008).
12. R. M. Smith, M. Bonati, and D. Guzman, "VIRGO-2K 2.25-μm HgCdTe dark current," *Proc. SPIE* **5499**, 119–130 (2004).

Biographies of the authors are not available.